Applied Catalysis B: Environmental 108–109 (2011) 90–99

Contents lists available at ScienceDirect

Applied Catalysis B: Environmental

journal homepage: www.elsevier.com/locate/apcatb

Ag/MCM-41 as a highly efficient mesostructured catalyst for the chemoselective synthesis of methyl glycolate and ethylene glycol

Anyuan Yin, Chao Wen, Wei-Lin Dai*, Kangnian Fan

Department of Chemistry and Shanghai Key Laboratory of Molecular Catalysis and Innovative Materials, Fudan University, Shanghai 200433, PR China

ARTICLE INFO

Article history:
Received 13 April 2011
Received in revised form 27 June 2011
Accepted 13 August 2011
Available online 19 August 2011

Keywords:
Ag/MCM-41
Dimethyl oxalate
Ethylene glycol
Methyl glycolate
Hydrogenation

ABSTRACT

A novel highly efficient heterogeneous Ag/MCM-41 catalyst was prepared by ammonia-evaporation deposition-precipitation method and displayed outstanding methyl glycolate (MG) selectivity (up to 99%) and ethylene glycol (EG) selectivity (up to 99%) in the chemoselective gas-phase hydrogenation of dimethyloxalate (DMO). Systematic characterizations have been carried out to elucidate the bulk and surface physicochemical properties of the catalysts. It is shown that the silver loading, the calcination temperature, the surface hydroxyl group amount and the pretreatment atmosphere all have great influences on the catalytic performance of DMO hydrogenation reaction. The best catalytic performance could be achieved over the Ag/MCM-41 catalyst with 10 wt.% silver loading after calcined at 673 K. Much higher catalytic activity could be obtained via the MCM-41 supported silver catalyst with large amount of surface hydroxyl groups. The argon pretreated Ag/MCM-41 catalyst with less subsurface oxygen species exhibited much higher DMO conversion and MG selectivity compared with H_2 and air pretreated samples. Under the optimized reaction conditions, 99% yield of MG and EG could be obtained over the optimized Ag/MCM-41 catalyst.

1. Introduction

The production of methyl glycolate (MG) and ethylene glycol (EG) is of industrial interest in the synthesis of polyesters as well as in the production of pharmaceutical products, fine chemicals and perfumes. Many approaches have been developed for the synthesis of MG and EG, however, severe reaction conditions and low yields of the target products make it hard to be applied in industry. As crude oil resources shrink, synthesis of MG and EG from syngas is attracting more and more interest. Alternative methods that proceed under mild reaction conditions with highly efficient and easy-to-handle heterogeneous catalysts are therefore economically and environmentally benign.

Supported silver catalyst is a kind of active material, which was widely used in catalytic oxidation reaction [1–6]; most well known is its industrial application for ethylene epoxidation and methanol oxidation to formaldehyde. However, silver can also be used as a catalyst for reductions, for example, selective hydrogenation of unsaturated aldehydes including acrolein, crotonaldehyde [7,8] and citral [9,10]. It was shown that small supported Ag particles favored the formation of allyl alcohol, which is likely related with the presence of electropositive sites like edges and kinks [7]. Defect site and subsurface oxygen have further been identified as an important factor influencing the selectivities in acrolein hydrogenation over silver catalyst [11,12]. Compared with the other metals such as nickel, palladium and platinum, silver is lack of affinity toward H_2 due to the filled d-band [13]. However, pretreatment of silver catalyst in O_2 would affect the interaction of silver with hydrogen. Theoretical calculations predict that silver atoms in the proximity of oxygen exhibit a higher affinity toward H_2 [12,14]. Experimental results show that the hydrogen adsorption capacity increases after a heat treatment in O_2 [15]. Moreover, oxygen impurities on the surface, which are difficult to remove [16], are believed to be responsible for the lower activation energy in the H_2–D_2-exchange reaction that is observed for granular silver in comparison with silver foil [13]. Recent studies show that O_2 pretreatment enhances the performance of supported silver catalysts in the hydrogenation of unsaturated aldehydes [11]. In addition, the amount of hydroxyl group has been found to have great influence on the catalytic oxidation behavior of silver catalyst [17].

In our previous work, it was found that high yields of MG and EG could be obtained over a novel Ag/SiO_2 catalyst via regioselective hydrogenation of dimethyloxalate (DMO) only by tuning the reaction temperature [18]. However, the supports of the catalysts used were different not only in textural structure, but also in particle size and morphology, all of which may lead to deviation in their catalytic behaviors. It is essential to figure out whether it is the intrinsic nature of silica textural properties or pretreatment of the catalyst under different atmospheric conditions or the amount of hydroxyl

* Corresponding author. Tel.: +86 21 55664678; fax: +86 21 55665701.
E-mail address: wldai@fudan.edu.cn (W.-L. Dai).

0926-3373/$ – see front matter © 2011 Elsevier B.V. All rights reserved.
doi:10.1016/j.apcatb.2011.08.013

group that contributes to the high activity in the reaction. In recent years, MCM-41 type mesoporous silica materials have been found with great interests due to its extraordinarily regular structure, very narrow pore size distribution and large surface area (usually above 1000 $m^2 g^{-1}$) [19]. The arrangement of regular parallel pores in the MCM-41 type materials resembles in some way the honeycomb structure. The structural, adsorptive or catalytic properties could be modified by the introduction of different species by various techniques, including direct hydrothermal, template ion-exchange, grafting or impregnation methods.

New types of hydrogenation catalyst have been prepared by the embedding of small metal crystallites (e.g. Pt, Pd, Au or Ni) or immobilization of various metal containing organic ligands. Metal species can be introduced to the mesoporous silica materials by several methods. One of the simplest ways is the addition of metal salts to the solution containing surfactant and silica source molecules. This technique has been successfully applied in the preparation of Al, Mn, V, Co or Cu containing materials [20]. It has been established that the structural properties and nature of metal species are strongly related to the preparation conditions, including pH of the solution, temperature and the ratio of Si/metal [21]. The mechanism of the formation of such systems is still under debate. Metal cations in aqueous solution are coordinated by water molecules, inorganic ligands (e.g. ammonia or chlorides) or bounded with hydroxyl groups. The catalytic properties of silver containing mesoporous silica materials have not been extensively studied. However, most of them have been prepared by the impregnation method using silica support with silver nitrate and then direct decomposition of the precursor at elevated temperatures. Due to the larger silver particle size, much lower catalytic activity could be obtained. In the present study, a novel approach to synthesize meso-structured Ag/MCM-41 was firstly reported and the catalytic behavior of the catalyst was applied in the regioselective hydrogenation of DMO to MG and EG.

2. Experimental

2.1. Catalyst preparation

2.1.1. MCM-41

Mesoporous siliceous MCM-41 was prepared according to a well-established procedure delineated by Beck et al. [22] using TEOS as silica source and CTAB as template agent. Typically, the MCM-41 materials were prepared by dissolving 5.528 g of CTAB in 240 g of deionized H_2O under vigorous stirring for 3.5 h at room temperature. Then 21 ml of ammonia (26 wt.%) was added before the addition of 21.39 g of TEOS dropwisely. The solution mixture was then stirred at 300 K for 2.5 h. After that, the resulting solid was recovered by filtration, washed with deionized water, and dried at 373 K, followed by calcination at 823 K in air for 5 h to remove the residual organic template materials, yielding the final mesoporous MCM-41 materials.

2.1.2. Ag/MCM-41

Silver modified meso-structured Ag/MCM-41 catalysts were prepared by ammonia-evaporation deposition-precipitation method (AE). A typical procedure is as follows. A certain amount of $AgNO_3$ was dissolved in 172 ml of deionized water. 23 ml of 28 wt.% ammonia aqueous solution was added and stirred for 30 min at 333 K to form silver ammonia complex solution. Then a certain amount of MCM-41 was added to the above silver ammonia complex solution and stirred for another 4 h. The initial pH of the suspension was 11–12. The suspension was then preheated at 363 K to allow for the evaporation of ammonia and the decrease of pH and consequently, the deposition of sliver species on silica. When the pH value of the suspension was decreased to 7.0, the evaporation process was terminated. The filtrate was washed with deionized water three times and ethanol once and then dried at 373 K overnight. Then the precursors were calcined from 373 to 873 K for 4 h to investigate the effect of calcination temperature on the structure evolutions. For Ag/MCM-41 samples with different silver loadings, the calcinations temperature is 673 K.

Series of catalysts with different amounts of hydroxyl group were prepared by AE method by using the MCM-41 support with different hydroxyl group amounts obtained via calcining the as-synthesized MCM-41 at different temperatures. The catalyst was denoted as Ag/MCM-41-T, where *T* stands for different calcinations temperature (823, 923, 1023 and 1123 K) on MCM-41 support.

To investigate the influence of the pretreatment atmosphere on the catalytic behavior of the catalysts, Ag/MCM-41 samples with 10 wt.% Ag loading pretreated with air, hydrogen and argon atmosphere at 673 K for 4 h were also prepared, which were denoted as Ag/MCM-41-A, Ag/MCM-41-H and Ag/MCM-41-N respectively.

2.2. Catalyst characterization

BET surface area (S_{BET}) was measured using N_2 physisorption at 77 K on a Micromeritics Tristar 3000 apparatus. The pore size distributions were obtained from desorption isotherm branch of the nitrogen isotherms by using the Barreett–Joyner–Halenda (BJH) method. The powdered X-ray diffraction (XRD) patterns were collected on a Bruker D8 Advance X-ray diffractometer using nickel-filtered Cu Kα radiation ($\lambda = 0.15418$ nm) with a scanning angle (2θ) of 20–80°, a scanning speed of 2° min^{-1}, and a voltage and current of 40 kV and 40 mA, respectively. Elemental analysis with respect to Ag loading was performed using ion-coupled plasma (ICP) atomic emission spectroscopy on a Thermo Electron IRIS Intrepid II XSP spectrometer. Transmission electron microscopy (TEM) was performed on a JEOL JEM 2011 instrument with an operating voltage of 200 kV. Samples were dispersed in ethanol, and a drop of the obtained suspension was fixed on a microgrid covered with amorphous carbon film. Thermal gravimetric analysis (TG) curves were monitored on a Mettler Toledo 851e apparatus. UV–visible diffuse reflectance spectra (UV–vis DRS) were recorded on a Shimadzu 2401PC UV-visible spectrophotometer with an integrating attachment using $BaSO_4$ as the background standard.

Temperature-programmed reduction (TPR) profiles were obtained on a Tianjin XQ TP5080 auto-adsorption apparatus. 50 mg of the calcinated catalyst was outgassed at 473 K under Ar flow for 2 h. After cooling to room temperature under Ar flow, the in-line gas was switched to 5% H_2/Ar, and the sample was heated to 1073 K at a ramping rate of 10 K min^{-1}. The H_2 consumption was monitored by a TCD detector. X-ray photoelectron spectroscopy (XPS) experiments were carried out with a Perkin-Elmer PHI 5000C ESCA system equipped with a hemispherical electron energy analyzer. The Mg Kα ($h\upsilon = 1253.6$ eV) anode was operated at 14 kV and 20 mA. The carbonaceous C 1s line (284.6 eV) was used as the reference to calibrate the binding energies (BEs).

2.3. Activity test

The catalytic evaluation was conducted using a fixed-bed reactor. Typically, 2.0 g of catalyst (40–60 meshes) was packed into a stainless steel tubular reactor. Catalyst pre-reduction was performed at 573 K for 4 h with a ramping rate of 2 K min^{-1}. After cooling to the reaction temperature, 15 wt.% DMO (purity > 99%) in methanol and H_2 were fed into the reactor at a H_2/DMO molar ratio of 100 and a system pressure of 2.5 MPa. The reaction temperature was firstly set at 473 K and the room-temperature LHSV of DMO was 0.2 h^{-1}. The products were condensed, and analyzed

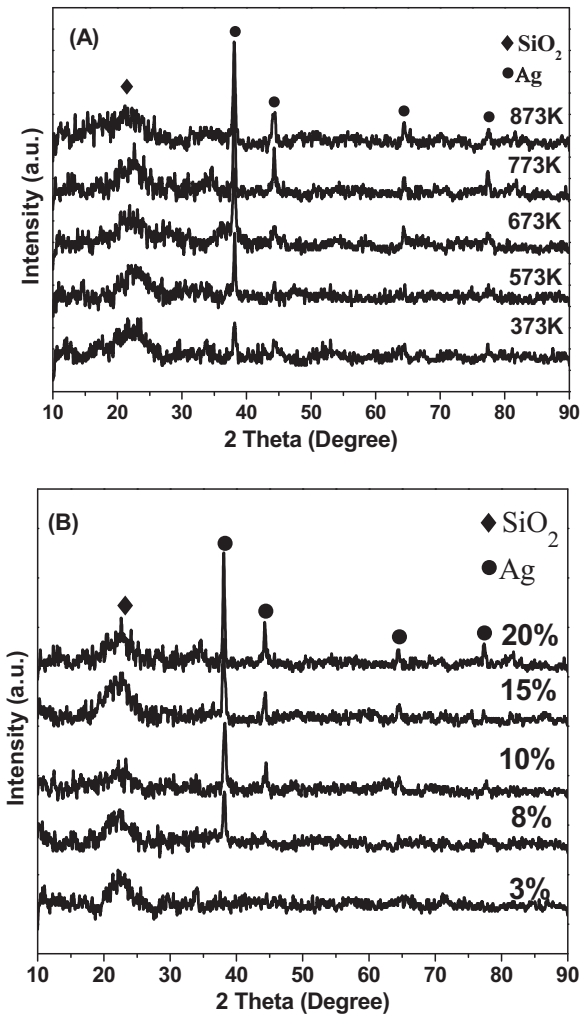

Fig. 1. (A) XRD patterns of Ag/MCM-41 catalyst with 10% Ag loading calcined at various temperatures. (B) XRD patterns of Ag/MCM-41 catalysts with various Ag loadings.

on a gas chromatograph (Finnigan Trace GC ultra) fitted with an HP-5 capillary column and a flame ionization detector (FID).

3. Results and discussion

3.1. Wide-angle XRD patterns

Fig. 1A shows the XRD patterns of Ag/MCM-41 catalysts with 10% Ag loading calcined at various temperatures. It clearly showed the appearance of the cubic phase of Ag with lattice constant $a = 4.0861$ Å (JCPDS: 65-2871), suggesting the presence of the metallic sliver particles in the samples. The four peaks appeared at $2\theta = 38.2^\circ$, 44.3°, 64.5° and 77.6°, which were ascribed to the (1 1 1), (2 0 0), (2 2 0) and (3 1 1) lattice planes of the metallic silver, especially those calcined at temperature higher than 673 K were very obvious. In addition, higher temperature calcinations would result in the growth of silver particles. Silver particle size calculated based on the XRD results (Table 1) showed that the higher treatment temperature would result in the larger particle size of silver, especially when the temperature was higher than 773 K.

Powdered XRD patterns of the Ag/MCM-41 catalysts with various Ag loadings are shown in Fig. 1B. All the samples were pretreated under air atmosphere at 673 K. No diffraction peaks of silver or silver compounds are observed on the 3% Ag/MCM-41 sample, indicating that silver species are well dispersed. XRD peak of metallic silver, especially the strongest one at $2\theta = 38^\circ$ corresponding to the (1 1 1) plane, appears in the high silver loading samples. The silver diffraction peaks became sharper and more obvious with the increase in silver loading. The particle size of silver catalyst calculated from the XRD results (Table 2) increases with the increase of the silver loading, and even the peak corresponding to Ag (3 1 1) at $2\theta = 77.6^\circ$ can be well resolved when the silver loading reaches 10%. The crystallite sizes, determined by Scherrer's equation from the XRD peak broadening, are 8.2, 9.7, 15.3, and 20.6 nm, respectively. The increased intensity of the Ag (1 1 1) peak may be caused by the increases in the amount of silver or the growth of silver particles. When the silver loading of the catalyst is higher than 15%, the average size of Ag particles does not change obviously.

3.2. Textural properties

The textual properties of the catalyst including the pore volume, pore diameter and BET surface area have profound influences on the catalytic behavior of the catalysts. To measure the effects of heat treatment and silver loading on the textural properties, the N_2 sorption and distribution of pore diameter were presented in Fig. 2.

Fig. 2(A) and (B) shows the N_2 adsorption–desorption isotherms and BJH pore size distributions of the Ag/MCM-41 samples with different silver loadings. As can be seen from Fig. 2(A), all the samples exhibited a typical adsorption curve of type IV, which is the characteristic of nanostructured materials with uniform mesopores. The adsorption and desorption isotherm showed a large increase in the relative pressure (P/P_0) range from 0.4 to 0.9, which is due to the capillary condensation of nitrogen within the mesopores. In addition, the silver loading was found to have a great effect on the distribution of the pore size. Three kinds of pores could be seen obviously at 2.4, 3.9 and 4.4 nm. As the increase of silver loading (lower than 15%), the distribution of the pore diameters did not shift much, suggesting that most of the silver particles are highly and uniformly dispersed in the inner pores of the MCM-41 or on the surface of the support. This finding could be further proved by the TEM images of the material in the following section. On the other hand, the decrease of the pore size indicated the decrease of the average pore volume as the increase of the silver loading, which might be due to the fulfillment of the silver particle into the pore of the support. It is worth noting that when the silver loading was higher than 15%, the smaller sized pores disappeared, implying that the excess amount of silver will fulfill or cover the small pores.

The physicochemical properties of catalysts with different silver loadings were summarized in Table 1. The actual silver loading measured by ICP is almost the same as the as-added amount within the experimental errors when the silver loading is lower than 15%. However, no obvious increase could be seen in silver loading with the further increase of the silver amount, which indicated that the saturate amount of silver on the MCM-41 support prepared by AE method was about 15 wt.%. It is obvious that the excess amount of silver would be washed away during the catalyst preparing procedure. The BET surface area and the pore volume decreased from 561 to 177 $m^2\,g^{-1}$ and from 0.80 to 0.35 $cm^3\,g^{-1}$ respectively as the increase of the silver loading, which might be resulted from the occupation of the silver particles into the pores or on the surface of the support. The average pore diameter increased from 5.7 to 7.6 nm as the increase of the silver loading from 3% to 20%, suggesting the decreased amount of the smaller pores which was in accord with the pore distribution shown in Fig. 2(B). The inconsistency of the average pore diameter and the pore diameter obtained from the pore size distribution curve might be originated from the macropores generated by the accumulated particles.

Table 1
The physicochemical properties and catalytic performance of Ag/MCM-41 catalysts with different silver loadings.

Silver loading (%)	Ag content (wt.%)	Ag_{surf} (%)[a]	d_{Ag} (nm)[b]	S_{BET} ($m^2\ g^{-1}$)	V_{pore} ($cm^3\ g^{-1}$)	D_{pore} (nm)	Y_{MG} (%)[c]	Y_{EG} (%)[d]	TOF (h^{-1})[e]
3	3.2	3.1	–	561	0.80	5.70	41	8	2.97
8	7.1	4.7	8.2	543	0.48	6.06	73	72.	2.00
10	10.0	5.9	9.7	266	0.46	6.37	90	99	1.92
15	12.3	10.4	15.3	212	0.37	6.50	73	65	1.13
20	13.5	10.9	20.6	177	0.35	7.63	59	59	1.04

[a] The surface silver loading, Ag_{surf}% was calculated by the surface Ag to Si atomic ratio obtained from the XPS spectra.
[b] Silver particle size was calculated by Scherrer's equation based on the XRD result.
[c] The yield of MG is obtained at 493 K.
[d] The yield of EG is obtained at 553 K.
[e] TOF = moles of DMO converted per moles of surface sliver amount based on XPS results in the catalyst per hour.

Table 2
The physicochemical properties and catalytic performance of 10% Ag/MCM-41 catalysts calcined at different temperatures.

Calcined temperature (K)	d_{Ag} (nm)[a]	Ag_{surf} (%)[b]	S_{BET} ($m^2\ g^{-1}$)	V_{pore} ($cm^3\ g^{-1}$)	D_{pore} (nm)	Y_{MG} (%)[c]	Y_{EG} (%)[d]	TOF (h^{-1})[e]
373	4.6	9.5	261	0.42	6.13	–	–	–
573	6.5	9.4	268	0.42	6.14	42	79	1.44
673	9.7	5.9	266	0.46	6.37	90	99	1.92
773	11.2	5.4	239	0.43	6.72	78	69	1.56
873	15.7	4.0	228	0.41	6.74	11	61	0.30

[a] Determined by Scherrer's equation based on XRD results.
[b] The surface silver loading, Ag_{surf}% was calculated by the surface Ag to Si atomic ratio obtained from the XPS spectra.
[c] The yield of MG is obtained at 493 K.
[d] The yield of EG is obtained at 553 K.
[e] TOF = moles of DMO converted per moles of surface sliver amount based on XPS results in the catalyst per hour.

As shown in Fig. 2(C), no obvious difference in the isotherm curve of the N_2 sorption could be found on the samples calcined at different temperatures, suggesting that the calcination temperature lower than 873 K has little influence on the pore structure of the materials. This finding could be further proved by the pore size distribution of the samples (Fig. 2(D)). Additional larger pore at 10.1 nm would appear when the treatment temperature was higher than 673 K, implying the collapse of the pores would occur at much higher calcination temperature.

The physicochemical properties of the samples at different calcination temperatures were summarized in Table 2. As can be seen, no obvious decrease in the BET surface area and the pore volume could be observed, which is in line with the N_2 sorption isotherms. Also the increase in average pore diameter is not obvious as the increase of the calcinations temperature. Combined with the XRD results, it could be concluded that the calcination temperature had more obvious influence on silver particle size than that on the textural structures of the catalyst.

3.3. TEM results

Fig. 3 shows the TEM image for the MCM-41 support and 10 Ag/MCM-41 sample. It shows clearly the hexagonal pore arrangement of the as-synthesized MCM-41 (Fig. 3A). After introducing the silver species, the hexagonal structure still retained (Fig. 3B and C), which indicated that the present preparation method had little effect on the uniform structure of MCM-41. It is also found that the size of the silver particle is around 10 nm which is in well accord with the XRD results. In addition, the silver particles exhibited spherical shape and homogeneously dispersed in the pores or on the surface of the support, which inhibited the aggregation of the silver nano-particles.

3.4. UV–vis DRS

Optical properties of solid materials are closely related to the microstructure, such as electronic state, defect sites, and energy level structure. Fig. 4 shows the UV–vis DRS spectra of samples with different silver loadings (Fig. 4A) and samples calcined at different temperatures (Fig. 4B). It is commonly accepted that the absorption band at 250 nm is ascribed to the isolated Ag^+, 290 nm to $Ag_n^{\delta+}$ and 400 nm to silver nano-particles [23–25]. It can be seen that the Ag/SiO_2 samples present a significant absorption in the visible region between 320 and 700 nm, which was attributed to the absorption of the silver surface plasmon. This absorption is due to collective oscillation of free conduction band electrons of the silver particles in response to optical excitation. For the sake of comparison, the UV–vis DRS spectra of samples with different silver loadings were shown in Fig. 4A. As the increase of silver loading, the intensity of the plasmon absorbance band also increased, which might be affected by the silver particle size, shape, the content of silver, and the surrounding chemical environment. The red shift as the increase of the silver loading might be the result of the size-dependent quantum confinement effect. In addition to the absorption in the visible region, the absorption in the UV region could also be observed, indicating that there is Ag^+ and $Ag_n^{\delta+}$ species on the surface of the samples. The existence of oxidative silver species suggested the presence of strong interaction between silica support and the silver species. Other research groups also reported that one peak at 250 nm assigned to the isolated Ag^+ species was observed with silver content of 10 or 20 wt.% [23]. Therefore, the UV–vis DRS spectra unambiguously demonstrate that Ag^+ ions were actually produced in the calcined samples. This result is in excellent agreement with the data from TPR and XPS as shown below.

To investigate the effect of calcinations temperature on the surface silver species, UV–vis DRS of samples calcined at different temperatures from 373 to 873 K was presented in Fig. 4B. No obvious shift of the absorption peak could be observed in both visible and UV region. The red-shift is connected with the growth of the nano particles, while the blue-shift is caused by the strong quantum confinement effect, suggesting that the size of silver particles are in the nanoscale. No obvious absorption peak at 259 and 295 nm could be found at the samples calcined at lower temperature (373 and 573 K), indicating the oxidative silver species formed at a certain higher temperature (higher than 573 K). The higher calcinations temperature is helpful to improve the interaction between silver species and silica support, thus to improve the

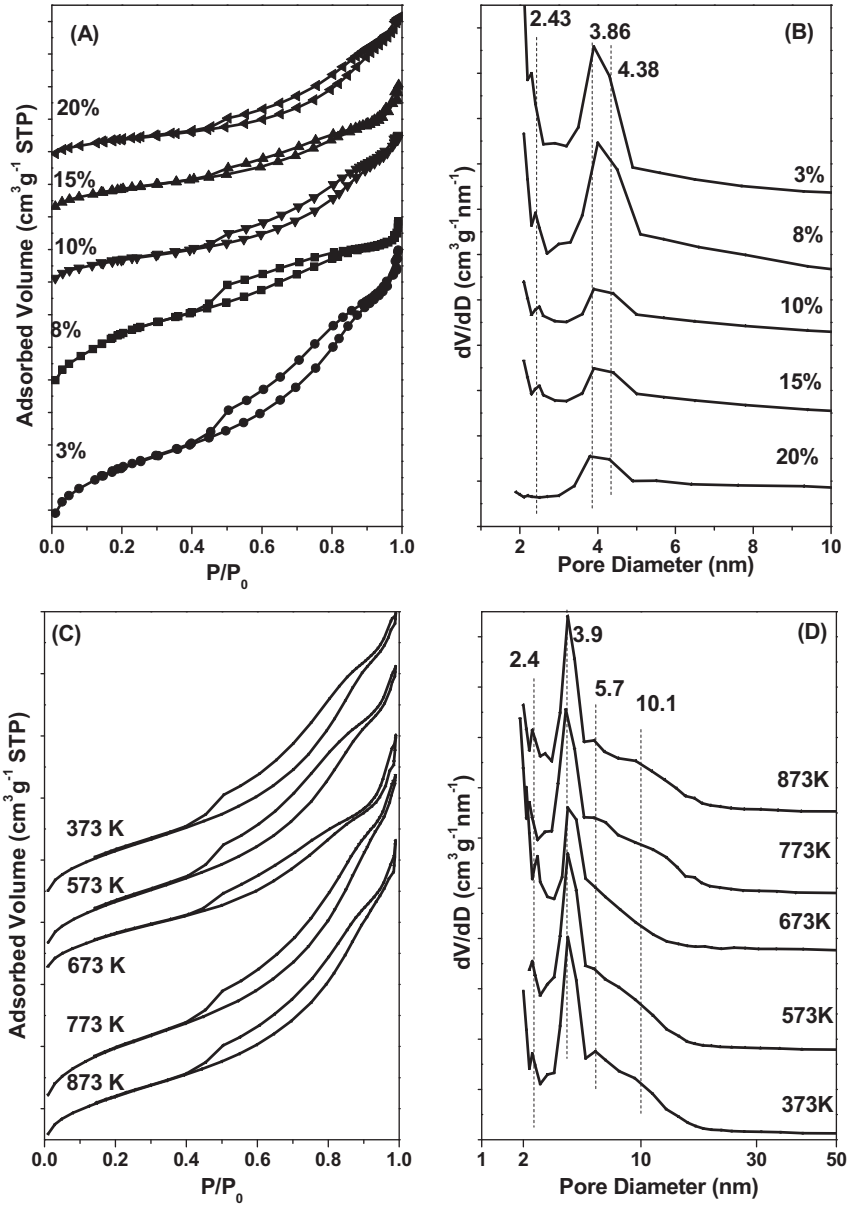

Fig. 2. N_2 adsorption–desorption isotherms of (A) the Ag/MCM-41 catalysts with various Ag loadings; (B) BJH pore size distribution of the Ag/MCM-41 catalysts with various Ag loadings; (C) N_2 adsorption–desorption isotherms of the Ag/MCM-41 catalysts with 10% Ag loading calcined at different temperatures; and (D) BJH pore size distribution of the Ag/MCM-41 catalysts with 10% Ag loading calcined at different temperatures.

dispersion of silver species. This finding is well consistent with the XPS and TPR results discussed in the context.

3.5. Redox properties of the Ag/MCM-41 samples

H_2-TPR is a very useful technology to investigate the redox properties and phase composition of the catalysts. The H_2-TPR profiles of series of samples with different silver loadings are shown in Fig. 5. As can be seen, each sample exhibits four hydrogen consumption peaks and the shapes of the peaks differ from each other. These findings indicate that at least two silver species are present in each sample. Based on the synthetic process (calcined under air atmosphere) combining with UV–vis DRS and XPS characterizations, the peaks centered at 370, 406, 420 and 462 K could be attributed to the reduction of Ag_2O, AgO, Ag_2O (formed by the reduction of AgO) and Ag_2SiO_3, respectively. The affinity of silver toward oxygen is well known [26,27], and a variety of oxygen species dissolved in the bulk, in the subsurface region, and on the surface of silver have been described elsewhere [26–28].

3.6. Surface chemical states of the Ag/MCM-41 samples

In order to investigate the chemical state of the silver species, the Ag 3d photoelectron spectra of samples with different Ag loadings as well as that of samples calcined at different temperatures were presented in Fig. 6. All the samples with different Ag loadings (Fig. 6A) showed an Ag 3d peak at 368.2 eV, which is in accordance with the binding energy value for a silver foil obtained by Waterhouse et al. [29] and was attributed to Ag^0. As the increase of the Ag loading, the BE of the Ag $3d_{5/2}$ shifted to the higher end, indicating that oxidized silver species also existed besides the metallic ones. For samples calcined at different temperatures, the BE of Ag $3d_{5/2}$ first decreased as the increase of the calcinations temperature, then increased as continuous increase of the calcinations temperature, suggesting the great influence of the calcinations temperature on

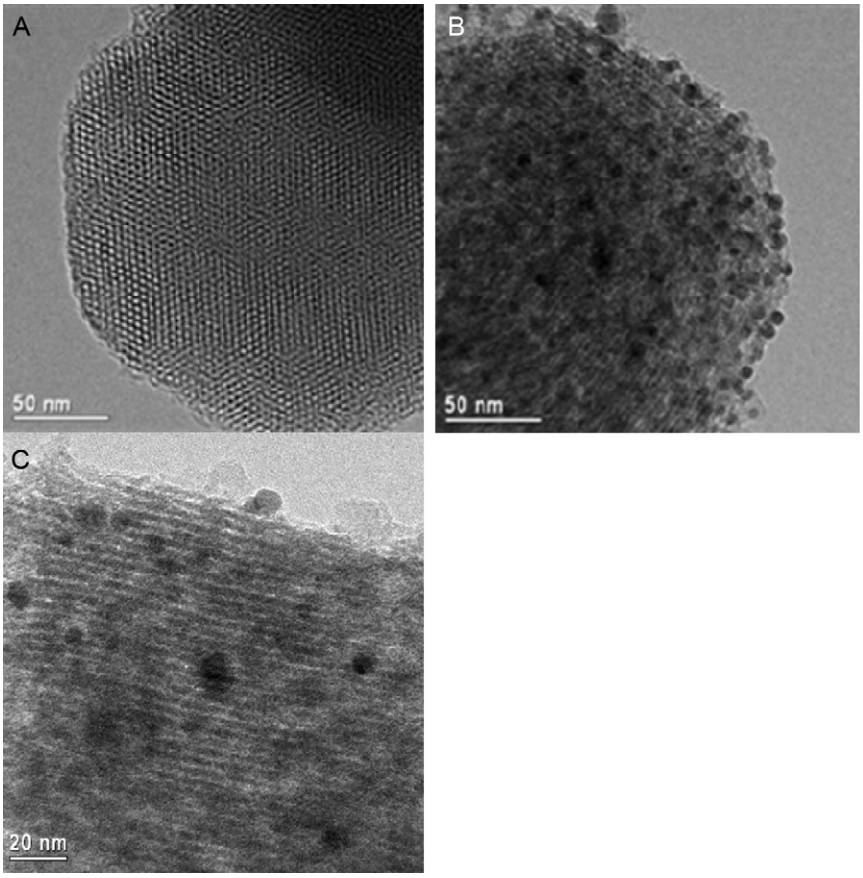

Fig. 3. TEM image of (A) MCM-41 support; and (B and C) 10 Ag/MCM-41 catalyst calcined at 673 K.

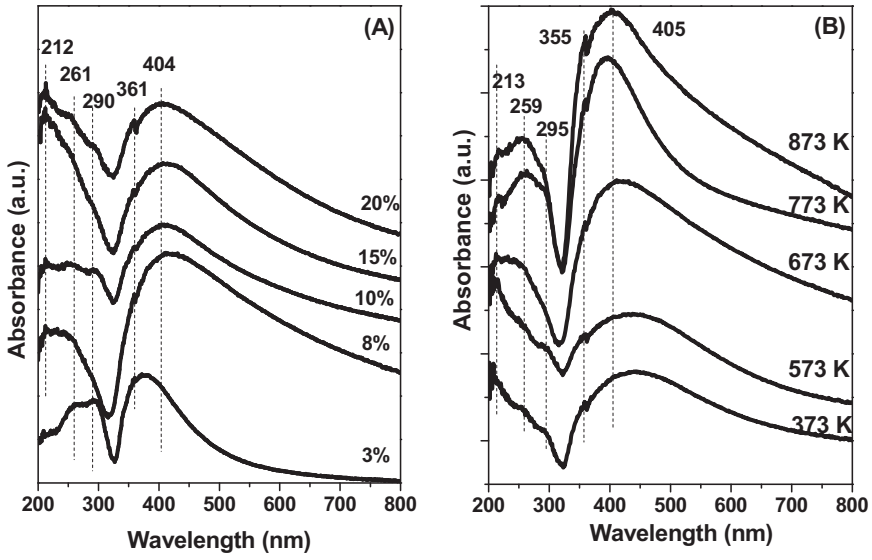

Fig. 4. UV–vis DRS of (A) samples with different Ag loadings and (B) samples calcined at different temperatures.

the chemical state of the silver species. When the calcination temperature was increased from 373 to 673 K, the BE of the Ag $3d_{5/2}$ decreased from 368.5 to 368.2 eV, indicating the oxidative silver species were formed during the higher temperature treatment process. However, continuous increasing the calcinations temperature would strengthen the interaction between silver species and the support, thus leading to the increase of the BE of silver $3d_{5/2}$. Due to the fact that the BEs are very close for each other and it is difficult to determine the oxidation state of the Ag particles, an additional study was performed on Ag MNN Auger spectra [30]. Fig. 6C shows Ag MNN Auger spectra of the samples calcined at different temperatures. Besides a peak at 358.2 eV which was attributed to the metallic Ag species, there is another peak at 355.6 eV assigned to the oxidative silver species, indicating that metallic silver and oxidative silver coexisted on the surface of the catalyst.

The use of XPS intensity ratios of metals to that of the support provides information regarding the dispersion degree of the active metals on the support. The results of the XPS intensity ratios of

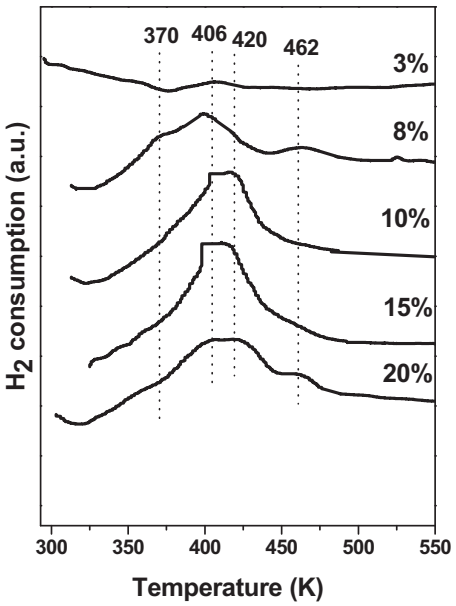

Fig. 5. H_2-TPR profiles of Ag/MCM-41 catalysts with different Ag loadings.

Ag/Si as a function of silver content as well as calcinations temperature are presented in Tables 1 and 2. As shown in Table 1, it is not surprising to find that the surface silver content increased steadily with the increment of silver loading up to 15%. The surface silver content was lower than that of the bulk and reached a maximum value at a certain silver loading because of the surface saturation, indicating that there is no Ag enrichment on the surface of the catalyst. Based on XPS and ICP analysis, the Ag/Si atomic ratio, the surface Ag/Si ratio and the silver loading were determined, and these values are also given in Table 1. Clearly, all the silver species were homogeneously dispersed on the surface of the support when the silver content was 3 wt.%. Higher silver loading would lead to the aggregation of the silver particles, thus resulted in the larger particle size. In addition, the surface silver content at 20% silver loading is only slightly higher than that of the 15% one, suggesting the Ag/SiO_2 catalyst reached surface silver saturation at 15% silver loading. In such a surface-saturated Ag/SiO_2 catalyst, silver particles were closely packed and could congregate easily, leading to the increased particle size, as confirmed by XRD results and TEM images.

It is worth noting that the surface content of silver species decreased from 9.5% to 4.0% as the increment of calcinations temperature from 373 to 873 K, suggesting that the higher temperature would lead to the migration of silver species from the surface to the bulk, which was in accordance with the result in literature [31]. Also, it could be originated from the particle growth, which resulted in lower XPS signals since penetration depth of X-rays in Ag is limited. The higher calcinations temperature would remove the surface OH group and eliminate the microholes by densification of the catalyst, thus might result in the lower Ag/Si ratio. On the other hand, the aggregated silver particles under higher calcinations temperature would also block part of the pores, thus was not convenient for the transferring of the reaction substrate.

3.7. TG profile

To investigate the influence of hydroxyl group amounts on the catalytic hydrogenation performance over silver catalysts. Supports with different hydroxyl group amounts were obtained via treating the support at different temperatures. Fig. 7 shows the TG profile of the MCM-41 support. As can be seen, the physical adsorption water could be removed at 523 K while the chemical bonded water could be removed until 1123 K. When the MCM-41 support was treated at 823, 923, 1023 and 1123 K, the weight loss due to the chemical dehydration could be up to 7%, 9%, 11% and 11% respectively, which was correspondent to the loss of different hydroxyl group amount.

3.8. Catalytic evaluation

3.8.1. Effect of Ag loading on the catalytic performance of DMO hydrogenation

DMO hydrogenation reaction was carried out to investigate the catalytic properties of Ag/MCM-41 catalysts, and their DMO conversion and production selectivity as a function of reaction temperature were shown in Fig. 8. It is not surprising to find that all the

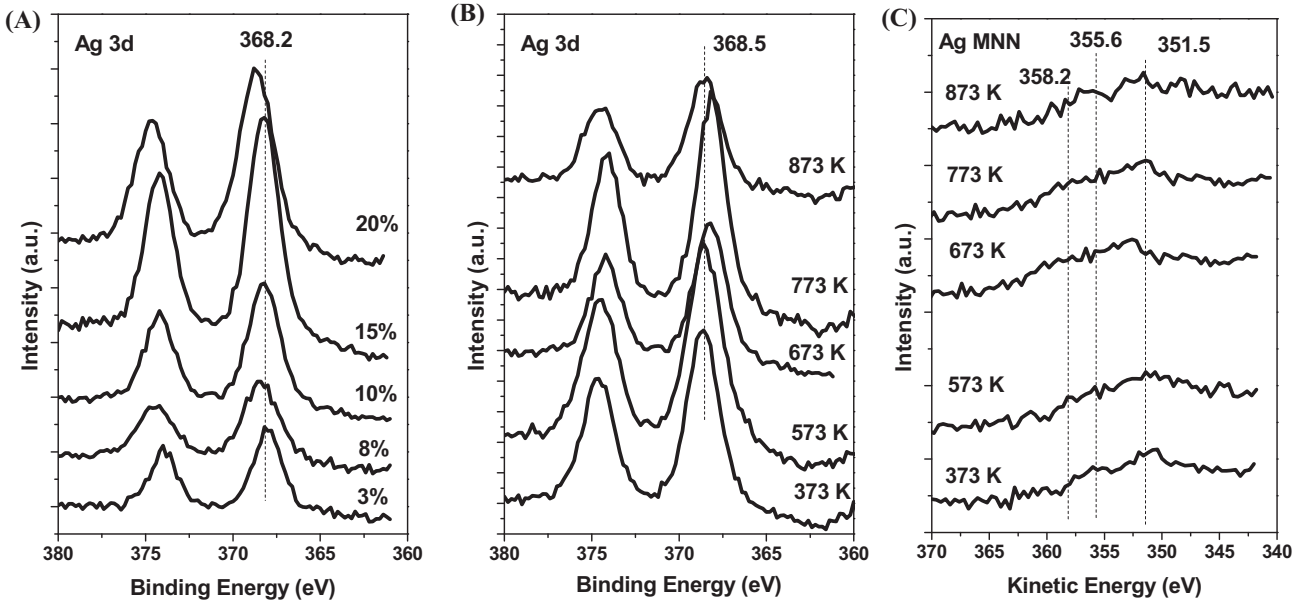

Fig. 6. Ag 3d XPS spectra of (A) catalysts with various Ag loadings; (B) 10 Ag/MCM-41 catalysts with different calcination temperatures; and (C) Ag MNN Auger spectra of 10 Ag/MCM-41 catalysts at different calcination temperatures.

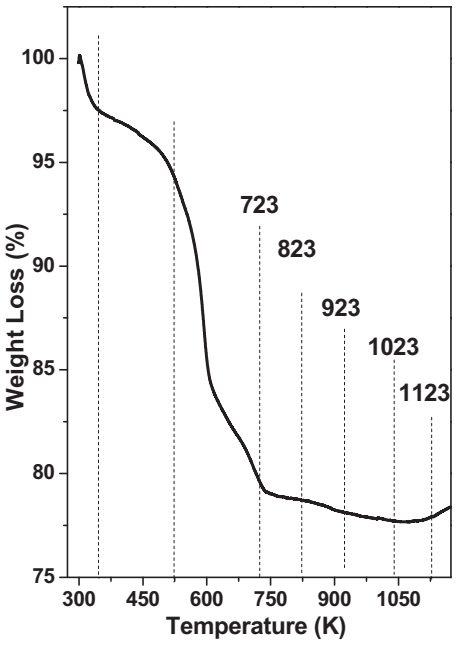

Fig. 7. TG profile of MCM-41 support.

catalysts with different Ag loadings exhibited excellent catalytic activity at higher reaction temperature (573 K) and the activity increased as the increment of the reaction temperature. Among those catalysts with different Ag loadings, the catalyst with 10% Ag loading presented the best catalytic activity not only at lower reaction temperature (473 K) but also at higher reaction temperature (573 K). In addition, the catalytic activity almost kept at a constant value when the reaction temperature increased from 493 to 573 K, indicating the highly thermal stability of the silver catalyst. At the same reaction temperature, taking 493 K for an example, the catalytic activity was in the following sequence: 10 Ag/MCM-41 = 15 Ag/MCM-41 > 8 Ag/MCM-41 > 20 Ag/MCM-41 > 3 Ag/MCM-41.

The selectivity to MG and EG could be controlled by adjusting the reaction temperature. Lower reaction temperature was helpful to selectively generate MG, whereas higher reaction temperature was tend to generate EG. It was noted that the catalyst with 3% silver loading exhibited higher selectivity to MG from lower to higher temperature. The selectivity to MG over other catalysts with silver loading higher than 3% presented a variation of reverse "S" shape, whereas the selectivity to EG of these catalysts showed a variation of "S" shape. The highest selectivity to MG and EG could be up to 95% and 99% at 493 and 553 K respectively.

3.8.2. Effect of the calcinations temperature on the catalytic performance of DMO hydrogenation

The catalytic performance was also examined via the catalyst with 10% silver loading to demonstrate the effect of calcinations temperature. The results are summarized in Table 2 and Fig. 8B. The maximum yield of MG and EG could be obtained over the same Ag/MCM-41 catalyst with 10% silver loading calcined at 673 K, which demonstrated the 10% Ag/MCM-41catalyst was highly efficient. The catalyst dried at room temperature was inactive at all reaction temperatures. The activity increased with increasing calcinations temperature owing to the reduction of silver ions. However, a very high calcinations temperature (773 K) diminished the activity, possibly due to the severe agglomeration of silver particles. It is found that the selectivity versus calcinations temperature plot shows a typical volcano shape with the highest value obtained at 673 K, which is determined to be the optimum calcinations temperature for achieving the highest MG and EG yield.

3.8.3. Effect of the hydroxyl group amounts on the catalytic performance of DMO hydrogenation

Qu et al. [17] reported an interesting finding that the catalytic performance of supported Ag/SiO_2 catalysts toward the selective oxidation of CO in the presence of excess amount of hydrogen at low temperatures could be greatly enhanced by pretreating the SiO_2 support before catalyst preparation. They thought that calcination of SiO_2 at appropriate temperature preferentially removed the H-bonded SiOH, which resulted in the highly dispersive Ag/SiO_2 catalyst and thus improved the catalytic performance. As the increase of the support treatment temperature from 923 to 1123 K, the BET surface area (S_{BET}) and the average pore volume (V_p) decreased severely from 460 to 10 $m^2\,g^{-1}$ and 0.39 to 0.03 $cm^3\,g^{-1}$ respectively, especially the catalyst pretreated at temperature higher than 1023 K, while the average pore diameter increased from 4.6 to 22.8 nm, which indicated that the collapse and destruction of the pore structure happened under the higher treatment temperature due to the excess loss of the water in the sample itself. The lower surface area will lead to bad dispersion of the silver species (the nature of oxidative silver species) on the surface of the catalyst, thus the larger silver nanoparticles would be formed due to the segregation effect. All these factors would have an adverse influence on the catalytic performance of the hydrogenation of DMO. To further investigate the influence of surface hydroxyl group amount on the catalytic hydrogenation performance, catalysts with different hydroxyl group amount were prepared and the results were presented in Fig. 8C. As shown in Fig. 8C, the catalytic activity decreased remarkably as the decrease of the surface hydroxyl group amount. For the catalyst Ag/MCM-41-1123, only 20% DMO conversion could be obtained even the reaction temperature was increased to 573 K, however, the selectivity to MG is nearly 100% in the range of reaction temperature from 433 to 573 K. The best catalytic activity could be obtained over Ag/MCM-41-823 catalyst, however, the selectivity to MG and EG exhibited an S-trend, which indicated the hydrogenation reaction was a continuous process, first DMO hydrogenated to MG, and then MG hydrogenated to EG.

3.8.4. Effect of the pretreatment atmospheres on the catalytic performance of DMO hydrogenation

The nature of active sites in silver catalysis remains controversial. Some researchers claimed that the existence of silver cations contributes to the high activity, whereas others insist that metallic silver species play an important role in obtaining highly catalytic performance. The affinity of silver toward oxygen is well known [27], and a variety of oxygen species dissolved in the bulk, in the subsurface region, and on the surface of silver have been well described [27]. Interaction of hydrogen with silver and support in Ag/SiO_2, Ag/Al_2O_3 and Ag/TiO_2 catalysts has also been described in the literature, including H_2 chemisorption on Ag/TiO_2 [32], kinetics of H_2/D_2 exchange on Ag/Al_2O_3 [33], H_2-promoted ethane isotopic homoexchange on Ag/SiO_2 [34], hydrogenation of ethane on Ag/SiO_2 and selective hydrogenation of α,β-unsaturated aldehydes [35,36].

To study the effects of pretreatment atmosphere on the catalytic performance of DMO hydrogenation, three kinds of 10 Ag/MCM-41 catalysts pretreated under air, H_2 and Ar were prepared. The DMO conversion, selectivity to MG and EG versus reaction temperature were presented in Fig. 8D. As can be seen, the DMO conversion of the Ar atmosphere pretreated sample was much higher than those of H_2 and air pretreated ones, especially at lower reaction temperature (lower than 473 K). However, no obvious difference in selectivity (both MG and EG) could be observed under the lower reaction temperature (lower than 473 K). For the three kinds of catalysts, lower reaction temperature is favorable to generate MG while the higher temperature is helpful to generate EG. The lower catalytic activity over air pretreated sample could be ascribed to the

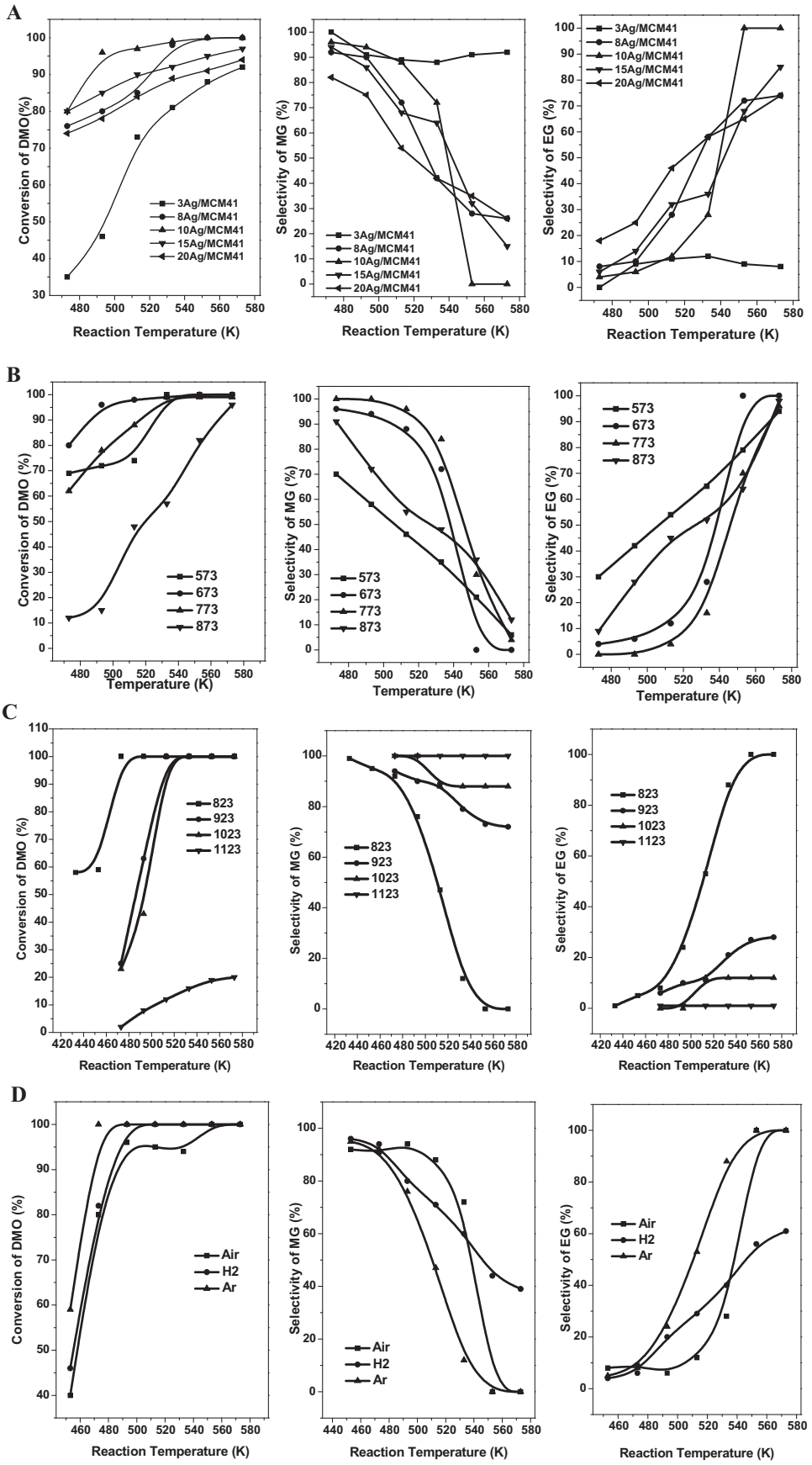

Fig. 8. DMO conversion profiles, MG selectivity profiles and EG selectivity profiles versus reaction temperature over (A) Ag/MCM-41 catalysts with various Ag loadings; (B) 10 Ag/MCM-41 catalysts with various calcination temperatures; (C) 10 Ag/MCM-41 catalysts with different hydroxyl group amounts; and (D) 10 Ag/MCM-41 catalysts pretreated under different atmospheres.

formation of the subsurface oxygen which was not active for hydrogenation reaction system. For H_2 and Ar pretreated silver catalysts, the surface oxygen might be destroyed, thus the higher hydrogenation performance could be obtained. The further insights on the detailed mechanism are still under way.

4. Conclusions

In summary, we have studied the catalyst system of Ag/MCM-41 synthesized via ammonia-evaporation deposition-precipitation method. Our findings indicate that the Ag loading, calcinations temperature, hydroxyl group amount and pretreatment atmosphere all have important influences on the catalytic performance of the selective hydrogenation of DMO. The best catalytic performance could be obtained over the catalyst with 10% silver loading and calcined at 673 K.

Acknowledgements

We thank the Major State Basic Resource Development Program (Grant Nos. 2003CB 615807), NNSFC (Project 21173052, 20973042), the Research Fund for the Doctoral Program of Higher Education (20090071110011) and the Science & Technology Commission of Shanghai Municipality (08DZ2270500) for financial support.

References

[1] O.V. Krylov, V.A. Matyshak, Russ. Chem. Rev. 64 (1995) 167.
[2] J.G. Serafin, A.C. Liu, S.R. Seyedmonir, J. Mol. Catal. A: Chem. 131 (1998) 157.
[3] A. Nagy, G. Mestl, T. Rühle, G. Weinberg, R. Schlögl, J. Catal. 179 (1998) 548.
[4] A. Nagy, G. Mestl, Appl. Catal. A 188 (1999) 337.
[5] A.J. Nagy, G. Mestl, R. Schlögl, J. Catal. 188 (1999) 58.
[6] J.R. Monnier, Appl. Catal. A 221 (2001) 73.
[7] M. Bron, D. Teschner, A. Knop-Gericke, F.C. Jentoft, J. Kröhnert, J. Hohmeyer, C. Volckmar, B. Steinhauer, R. Schlögl, P. Claus, Phys. Chem. Chem. Phys. 9 (2007) 3559.
[8] M. Bron, D. Teschner, A. Knop-Gericke, B. Steinhauer, A. Scheybal, M. Hävecker, D. Wang, R. Födisch, D. Hönicke, A. Wootsch, R. Schlögl, P. Claus, J. Catal. 234 (2005) 37.
[9] M. Steffan, M. Lucas, A. Brandner, M. Wollny, N. Oldenburg, P. Claus, Chem. Eng. Technol. 30 (2007) 481.
[10] M. Steffan, M. Lucas, A. Brandner, P. Claus, M. Wollny, N. Oldenburg, Chem. Ing. Technol. 78 (2006) 923.
[11] M. Bron, D. Teschner, U. Wild, B. Steinhauer, A. Knop-Gericke, C. Volckmar, A. Wootsch, R. Schlögl, P. Claus, Appl. Catal. A 341 (2008) 127.
[12] A.B. Mohammad, I.V. Yudanov, K.H. Lim, K.M. Neyman, N. Rösch, J. Phys. Chem. C 112 (2008) 1628.
[13] R.J. Mikovksy, M. Boudart, H.S. Taylor, J. Am. Chem. Soc. 76 (1954) 3814.
[14] Y. Xu, J. Greeley, M. Mavrikakis, J. Am. Chem. Soc. 127 (2005) 12823.
[15] S.R. Seyedmonir, D.E. Strohmayer, G.J. Guskey, G.L. Geoffroy, M.A. Vannice, J. Catal. 93 (1985) 288.
[16] F.H. Buttner, E.R. Funk, H. Udin, J. Phys. Chem. 56 (1952) 657.
[17] Z.P. Qu, W.X. Huang, S.T. Zhou, H. Zheng, X.M. Liu, M.J. Cheng, X.H. Bao, J. Catal. 234 (2005) 33.
[18] A.Y. Yin, X.Y. Guo, W.L. Dai, K.N. Fan, Chem. Commun. 46 (2010) 4348.
[19] A. Corma, Chem. Rev. 97 (1997) 2373.
[20] W.H. Zhang, X.B. Lu, J.H. Xiu, Z.L. Hua, L.X. Zhang, M. Robertson, J.L. Shi, D.S. Yan, J.D. Holmes, Adv. Funct. Mater. 14 (2004) 544.
[21] H.P. Lin, C.Y. Mou, Acc. Chem. Res. 35 (2002) 927.
[22] J.C. Vartuli, K.D. Schmitt, C.T. Kresge, W.J. Roth, M.E. Leonowicz, S.B. McCullen, S.D. Hellring, J.S. Beck, J.L. Schlenker, Chem. Mater. 6 (1996) 2317.
[23] K. Shimizu, A. Satsuma, Phys. Chem. Chem. Phys. 8 (2006) 2677.
[24] K. Shimizu, J. Shibata, H. Yoshida, A. Satsuma, T. Hattori, Appl. Catal. B 30 (2001) 151.
[25] Z. Li, M. Flytzani-Stephanopoulos, J. Catal. 182 (1999) 313.
[26] C. Rehren, G. Isaac, R. Schlögl, G. Ertl, Catal. Lett. 11 (1991) 253.
[27] A.J. Nagy, G. Mestl, D. Herein, G. Weinberg, E. Kitzelmann, R. Schlögl, J. Catal. 182 (1999) 417.
[28] B. Pettinger, X. Bao, I.C. Wilcock, M. Muhler, G. Ertl, Phys. Rev. Lett. 72 (1994) 1561.
[29] G.I.N. Waterhouse, G.A. Bowmaker, J.B. Metson, Appl. Surf. Sci. 183 (2001) 191.
[30] A. Naydenov, P. Konova, Pen. Nikolov, F. Klingstedt, N. Kumar, D. Kovacheva, P. Stefanov, R. Stoyanova, D. Mehandjiev, Catal. Today 137 (2008) 471.
[31] Z.P. Qu, W.X. Huang, M.J. Cheng, X.H. Bao, J. Phys. Chem. B 109 (2005) 15842.
[32] S.R. Seyedmonir, D.E. Strohmayer, G.L. Geoffroy, M.A. Vannice, H.W. Young, J.W. Linowski, J. Catal. 87 (1984) 424.
[33] H. Backman, J. Jensén, F. Klingstedt, J. Wärnä, T. Salmi, D.Y. Murzin, Appl. Catal. A 273 (2004) 303.
[34] V. Muzykantov, H. Ehwald, A. Shestov, N. Bogdanchikova, React. Kinet. Catal. Lett. 40 (1989) 31.
[35] P. Claus, P.A. Crozier, P. Druska, Fresenius J. Anal. Chem. 361 (1998) 677.
[36] P. Claus, H. Hofmeister, J. Phys. Chem. B 103 (1999) 2766.